Available online at www.sciencedirect.com
SCIENCE DIRECT®
Journal of Chromatography A, 1092 (2005) 149–160
JOURNAL OF CHROMATOGRAPHY A
www.elsevier.com/locate/chroma

Effect of pressure drop on solute retention and column efficiency in supercritical fluid chromatography

Arvind Rajendran[a], Oliver Kräuchi[a], Marco Mazzotti[a,*], Massimo Morbidelli[a,b]

[a] *ETH Swiss Federal Institute of Technology Zurich, Institute of Process Engineering, Sonneggstrasse 3, CH–8092 Zürich, Switzerland*
[b] *Institute for Chemical and Bioengineering, ICB, ETH Hönggerberg/HCI, CH-8093 Zurich, Switzerland*

Available online 5 July 2005

Abstract

The effect of pressure drop on the performance of supercritical fluid chromatographic systems is studied. Experiments have been conducted at different pressures and at 55 and 65 °C. Experiments at conditions leading to large and small pressure drops have been performed. Parameters to describe the pressure drop, retention time and efficiency have been extracted from these experiments. Using these parameters the dynamics of the chromatographic column have been modeled. Darcy's law was used to describe the pressure drop. The efficiency was modeled by considering the contributions from axial dispersion, resistance to mass transfer from the fluid film, and to diffusion in the pores. Good description of the pressure drop, retention time and mass transfer characteristics under normal operating conditions was obtained. The parameters extracted were used to predict the elution profile by numerical simulations. Considerable loss in column efficiency was observed when operating the column at lower values of the back pressure.

Keywords: Supercritical fluid chromatography; Pressure drop; Modeling; Efficiency; Simulation

1. Introduction

Supercritical fluids are tunable solvents, since their solvent power can be altered easily by changing the operating pressure. At conditions close to the critical point, they exhibit properties intermediate to those of liquids and gases, e.g., lower viscosity and higher diffusivity as compared to liquids. This and the fact that CO_2 is non-toxic, non-flammable, and benign, with mild critical temperature and pressure, has made it attractive for supercritical CO_2 to be used as solvent in chromatography. Supercritical fluid chromatography (SFC), which offers faster and more efficient separation as compared to high performance liquid chromatography (HPLC), has been increasingly used as a preparative tool for the separation of enantiomers for pharmaceutical applications [1]. Moreover, supercritical fluid-simulated moving bed (SF-SMB) processes have been developed and enantioseparations have been successfully performed [2,3].

SFC possesess characteristics different from HPLC that make its study challenging. In SFC the retention of a solute is influenced by the density of the mobile phase. The solute is more strongly retained at lower than at higher pressures. This stems from the fact that the solvent power of the supercritical fluid is weaker at lower than at higher pressure levels. Hence, at a given temperature, the effect of the operating pressure has to be studied to design an effective separation. The variation of the retention factor with the mobile phase pressure can be used to advantage in the SF-SMB process. Traditional SMB units have four sections, namely 1, 2, 3 and 4. Sections 2 and 3 are used for the separation of the solutes, while Sections 1 and 4 are used to regenerate the stationary phase and the solvent, respectively. The objective, hence, is to enforce conditions so that the solute is weakly retained in Section 1 and strongly retained in Section 4. This can be achieved by applying a pressure gradient, namely decreasing pressure levels going from Sections 1 to 4. It has been shown, both theoretically and experimentally, that operating a SF-SMB unit in the pressure gradient mode offers higher productivity as compared to the isocratic operation

* Corresponding author. Tel.: +41 44 632 2456; fax: +41 44 632 1141
E-mail address: marco.mazzotti@ipe.mavt.ethz.ch (M. Mazzotti).

0021-9673/$ – see front matter © 2005 Elsevier B.V. All rights reserved.
doi:10.1016/j.chroma.2005.06.047

[2,4]. In the reported experimental SF-SMB separation, the implementation of a pressure gradient was achieved by positioning a back pressure regulator in between Sections 2 and 3. Hence in the unit Sections 1 and 2 were at a higher pressure, whereas Sections 3 and 4 were at a lower pressure. Other possibilities of implementing the gradient are by introducing capillaries in between the columns, or by operating the SMB unit at a high flow rate so that the flow causes a natural pressure drop. Operating the chromatographic system at high enough flow rates, i.e., where pressure drop is large, will also be desired in single column preparative SFC systems where the emphasis would be on increasing throughput. However, close to the critical point, since the density of a supercritical fluid is a strong function of the pressure, operating the SFC under these conditions causes a density gradient across the column, hence corresponding variations of velocity, viscosity, diffusivity, and retention factor of the solute. Under these conditions, the response of an injected pulse is influenced by the variation of all these parameters and this has to be properly described to optimize the operation of preparative SFC and SF-SMB processes.

The effect of pressure drop on SFC performance has been studied in the past, while only a few studies have dealt with the modelling of these effects in packed column SFC [5–8]. In the current study, experimental data have been obtained over a range of operating conditions, which extends from low pressure drop ($\Delta P < 1$ bar) to high pressure-drop ($\Delta P \simeq 30$ bar) at two temperatures, 55 and 65 °C, using pure CO_2 as a mobile phase. These experiments involved the injection of a pulse of phenanthrene on a LiChrospher RP-18 column. Parameters to describe the hydrodynamics (ΔP), equilibrium (retention time, t_i^R), mass transfer (height equivalent to a theoretical plate, HETP) have been extracted from these experiments and were used to predict the performance of SFC systems at large pressure drop conditions.

2. Modeling approach

The ultimate goal of the study is to adapt the conventional model used to describe the dynamics of an adsorption column to SFC systems under non-negligible pressure drop conditions. The equations describing the hydrodynamics and the column dynamics are given below:

Hydrodynamics

Pressure drop relationship

$$\frac{dP}{dz} = -\beta\frac{(\rho v)\mu}{\rho} \quad (1)$$

Continuity equation

$$\frac{d(\rho v)}{dz} = 0 \quad (2)$$

Solute Propagation

Overall solute material balance

$$\frac{\partial c_i}{\partial t} = \frac{\partial}{\partial z}\left(D_{ax,i}(\rho)\frac{\partial c_i}{\partial z}\right) - \frac{\partial(c_i v)}{\partial z} - \frac{1-\epsilon_b}{\epsilon_b}\frac{\partial n_i}{\partial t} \quad (3)$$

Stationary phase material balance

$$\frac{\partial n_i}{\partial t} = k_i(n_i^* - n_i) \quad (4)$$

Adsorption isotherm

$$n_i^* = F(c_i, \rho) \quad (5)$$

Eq. (1), the well known Darcy's equation, describes the pressure drop in a packed column under laminar flow conditions, in terms of the viscosity, μ, density, ρ, interstitial velocity of the mobile phase, v, while β is a system dependent constant. Eqs. (1) and (2) are closed with a suitable Equation of State (EOS) and a constitutive equation that relates the fluid viscosity to the pressure and temperature. Eq. (3) describes the transport of a component i along the chromatographic column with c_i and n_i being its concentrations in the fluid and solid phase, respectively, while ϵ_b is the bed void fraction. Eq. (4) represents a linear driving force mass transfer model with k_i being the lumped mass transfer coefficient, and n_i^* being the concentration in the solid phase at equilibrium with the fluid phase concentration c_i. Eq. (5) specifies the general form of the adsorption isotherm. In this study the injected solute is rather dilute, so as its adsorption/desorption can be assumed not to affect the density and the related properties of the mobile phase. Owing to this assumption, the equations describing the hydrodynamics, i.e., Eqs. (1) and (2) can be decoupled from those describing the adsorption column dynamics, i.e., Eqs. (3)–(5). Hence, Eqs. (1) and (2), along with suitable boundary conditions, can be solved to yield the profiles of pressure, density, velocity and viscosity along the column. In addition, by using an appropriate correlation, the diffusivity of the solute in the solvent can be calculated as a function of temperature and density. These can then be used to solve the equations describing the solute propagation, by taking into account the local variations of the above mentioned properties along the column.

3. Experimental

3.1. Materials

Phenanthrene (purity >97%) and Toluene (purity >99.7%) were obtained from Fluka Chemie, Buchs, Switzerland. Carbon dioxide (99.995% pure) was obtained from PanGas AG, Luzern, Switzerland. A 125 mm long, 4 mm diameter LiChrospher RP-18 column (Merck Darmstadt, Germany) with 5 μm particles was used for all the experiments.

3.2. Experimental set-up

A scheme of the experimental set-up is shown in Fig. 1. The CO_2 from the cylinder is cooled and pumped to a desired pressure by an air-driven pump (Maximator, Amman-Technik AG, Köllikon, Switzerland). A constant flow of CO_2 is provided by a syringe pump (ISCO 260D, ISCO, Nebraska, USA), whose head is cooled to 15 °C. A motor driven injection valve (Valco C14W, Valco Instuments, Houston, TX, USA) with a 60 nL internal sample loop is used to inject a pulse into the column. Thin capillaries of 0.12 mm internal diameter, and of 5 and 8 cm length were introduced upstream and downstream of the column, respectively. The pulse response was measured using a UV detector (Jasco UV-1570, Omnilab AG, Mettmenstetten, Switzerland). The system pressure was controlled by a back pressure regulator (Jasco BP-1580-81, Omnilab AG, Mettmenstetten, Switzerland), with a control precision of 2% of the set value, and situated downstream of the UV detector. The column and the injection valve were housed in a temperature controlled water bath. Upstream and downstream pressures were measured using pressure transducers (Trafag-8891, Trafag AG, Maennendorf, Switzerland) at the locations shown in the figure.

At the start of an experiment, the back pressure regulator was set to the desired level and the syringe pump was programmed to provide a constant volumetric flow rate. The system was then allowed to reach steady state, i.e., the establishment of a time-invariant pressure profile. Once these conditions were reached, a pulse of a mixture of phenanthrene in toluene (2%, w/w) was fed using the injection valve; the data acquisition was started simultaneously. For each setting, the experiment was repeated at least three times to ensure reproducibility. The total porosity of the column was determined by injecting a sample of toluene at the highest pressure allowed ($\simeq$ 250 bar), assuming that toluene was not retained under the prevailing operating conditions. A value of 0.65 was obtained for the total porosity of the column, ϵ.

4. Pressure drop

Since the pressure profile in the column determines the profile of all physical parameters characterizing the column dynamics, care should be taken in characterizing pressure drop. In the SFC set-up shown in Fig. 1, pressure drop was measured across the injection valve, the capillaries, the column and the UV detector, where the contributions due to the injection value and the UV detector were negligible. Hence, the overall pressure drop, ΔP, was considered to arise from the column, ΔP_{col} and the capillaries, i.e., ΔP_{us} and ΔP_{ds}, the contribution of the capillaries located upstream and downstream of the column respectively. The later quantities were estimated by performing experiments where the column was replaced by a zero dead-volume connector giving negligible pressure drop. Under these conditions, in addition to measuring the pressure drop along the capillaries, pulse injections were also performed, thus estimating the dead time and the axial dispersion in the tubing that were later used to analyze the retention time and the HETP in the chromatographic column. The experimental pressure drop in the piping and the fittings present in the section of the equipment where the pressure drop was measured, was described using the Blasius equation written in terms of mass flow rate, G:

$$\frac{dP}{dz} = -\alpha \frac{G^{7/4}\mu^{1/4}}{\rho} \tag{6}$$

The parameter α, which is independent of the operating conditions, was obtained by fitting Eq. (6) to the pressure drop values obtained from the runs with the zero-dead volume connector at 65 °C, and a value of 3.211×10^8 cm$^{-19/4}$ was obtained. In this study the EOS proposed by Span and Wagner [9], and the correlation to calculate the viscosity of pure CO_2 proposed by Fenghour et al. [10] were used.

For the study of the effect of pressure drop in the chromatographic column, the pressure at the column inlet and outlet had to be obtained. This means that the pressure drop contribution of the capillaries must be subtracted from the total pressure drop measured across the capillaries and the column. To obtain the pressure at the inlet of the column, Eq. (6) along with the EOS and the correlation for estimating the viscosity was solved using P_{in} as pressure value at the inlet of the capillary. In order to obtain the pressure at the column outlet, the same equations were solved backwards, but with P_{out} as the pressure value at the outlet of the downstream capillary. These calculations yielded ΔP_{us} and ΔP_{ds} from which the pressure drop in the column, ΔP_{col}, was calculated. From this estimated value of ΔP_{col}, β in Eq. (1) was calculated by fitting the data of all the experiments performed at 65 °C thus obtaining $\beta = 2.54 \times 10^{10}$ cm^{-4}. Since the parameters α and β are independent of temperature, the values obtained at 65 °C were used to estimate pressure drops across the capillary at 55 °C. The estimated contributions of the individual capillaries and the column are summarized in Tables 1 and 2. The value of the back pressure reported in the table corresponds to the set point to the back pressure regulator, while P_{out}, is the pressure value measured downstream of the UV detector. The difference between the set point and P_{out} is due to the precision of the back pressure regulator.

In the operation of prep-SFCs and SF-SMB units under pressure gradient conditions, the parameters that are specified are the back-pressure and the mass flow rate. From these parameters the model should be able to estimate the pressure profile in the system. Hence, with the value of P_{out}, as a boundary condition, the total pressure drop in the system was calculated by appropriately using Eqs. (1) and (6), i.e.,:

$$\Delta P_{pred} = \Delta P_{ds}|_{pred} + \Delta P_{c}|_{pred} + \Delta P_{us}|_{pred} \tag{7}$$

The predicted values of the pressure drops are given alongside the experimentally measured values in Tables 1 and 2. It can be seen that the average difference between the predicted and experimental values was within 2.0 bar. This indicataes

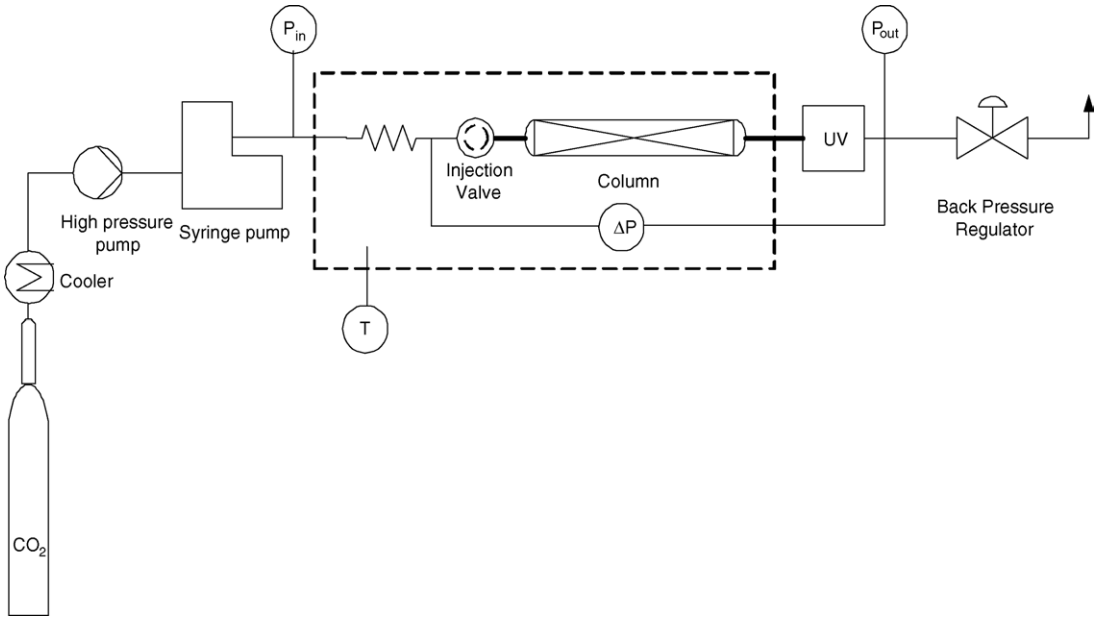

Fig. 1. Schematic of the SFC plant used in the study. Thick lines between the injection valve and column inlet and between column outlet and UV detector are capillaries with an internal diameter of 0.12 mm.

Table 1
Calculated values of pressure drops at 55 °C

Back pressure (bar)	P_{out} pressure (bar)	Flowrate ΔP_{us} at CO_2 pump (cm^3/min)	ΔP_{us} (bar)	ΔP_{col} (bar)	ΔP_{ds} (bar)	ΔP_{expt} (bar)	ΔP_{pred} (bar)
130	132.7	0.30	0.1	1.1	0.1	1.3	1.8
	132.8	0.50	0.2	2.0	0.4	2.6	3.2
	132.7	0.75	0.5	3.0	0.7	4.2	5.1
	132.4	1.00	0.8	4.2	1.2	6.2	7.2
	132.7	2.00	2.5	9.3	4.2	16.0	17.3
	132.8	3.00	5.0	15.5	8.6	29.1	30.0
	133.0	4.00	8.3	22.7	14.4	45.4	45.1
	133.4	5.00	12.2	31.0	21.4	64.6	62.6
150	152.9	0.30	0.1	1.2	0.1	1.4	1.9
	152.9	0.50	0.2	2.1	0.3	2.6	3.3
	152.9	0.75	0.4	3.2	0.7	4.3	5.3
	152.8	1.00	0.7	4.4	1.2	6.3	7.4
	152.9	2.00	2.5	9.6	4.0	16.1	17.7
	152.9	3.00	5.0	15.9	8.3	29.2	30.4
	153.1	4.00	8.2	23.2	13.9	45.3	45.6
	153.3	5.00	12.2	31.6	20.7	64.5	63.1
180	182.4	0.30	0.1	1.3	0.1	1.5	2.0
	182.6	0.50	0.2	2.2	0.3	2.7	3.5
	182.6	0.75	0.4	3.4	0.7	4.5	5.5
	182.6	1.00	0.7	4.6	1.2	6.5	7.8
	182.6	2.00	2.4	10.1	4.0	16.5	18.4
	182.8	3.00	5.0	16.6	8.1	29.7	31.4
	182.8	4.00	8.2	24.1	13.6	45.9	46.7
	183.3	5.00	12.2	32.6	20.3	65.1	64.4
210	212.8	0.30	0.1	1.4	0.1	1.6	2.1
	212.8	0.50	0.2	2.3	0.3	2.8	3.7
	212.8	0.75	0.4	3.6	0.7	4.7	5.8
	212.4	1.00	0.7	4.9	1.1	6.7	8.1
	212.4	2.00	2.4	10.6	3.9	16.9	19.0
	212.7	3.00	5.0	17.2	8.1	30.3	32.3
	213.0	4.00	8.3	24.9	13.5	46.7	48.0

ΔP_{us}: pressure drop in the capillaries located upstream of the column; ΔP_{col}: pressure drop across the chromatographic column; ΔP_{ds}: pressure drop across capillary located downstream of the column.

Table 2
Calculated values of pressure drops at 65 °C

Back pressure (bar)	P_{out} pressure (bar)	Flowrate ΔP_{us} at CO_2 pump (cm^3/min)	ΔP_{us} (bar)	ΔP_{col} (bar)	ΔP_{ds} (bar)	ΔP_{expt} (bar)	ΔP_{pred} (bar)
130	131.9	0.30	0.1	1.1	0.2	1.4	1.8
	131.9	0.50	0.3	1.9	0.4	2.6	3.2
	131.9	0.75	0.5	3.0	0.9	4.4	5.2
	131.0	1.00	0.9	4.2	1.5	6.6	7.4
	131.2	2.00	2.8	9.4	5.0	17.2	18.0
	132.9	3.00	5.5	15.7	10.0	31.2	31.2
	133.3	4.00	8.8	22.9	16.5	48.2	46.8
	133.4	5.00	12.9	31.3	24.3	68.5	64.8
150	152.3	0.30	0.1	1.2	0.2	1.4	1.8
	152.8	0.50	0.2	2.0	0.4	2.6	3.2
	152.8	0.75	0.5	3.1	0.8	4.4	5.2
	151.8	1.00	0.8	4.2	1.3	6.3	7.4
	151.8	2.00	2.7	9.5	4.5	16.7	17.8
	152.0	3.00	5.3	15.8	9.1	30.2	30.8
	152.4	4.00	8.7	23.1	15.2	47.0	46.2
	153.0	5.00	12.7	31.5	22.5	66.7	64.0
180	182.6	0.30	0.1	1.2	0.2	1.5	1.9
	182.7	0.50	0.2	2.1	0.4	2.7	3.4
	182.7	0.75	0.5	3.3	0.7	4.4	5.4
	182.6	1.00	0.8	4.5	1.2	6.5	7.6
	182.6	2.00	2.6	9.9	4.2	16.7	18.7
	182.5	3.00	5.2	16.3	8.6	30.1	31.2
	182.8	4.00	8.6	23.7	14.4	46.7	46.6
	182.9	5.00	12.6	32.1	21.5	66.2	64.4
210	212.6	0.30	0.1	1.3	0.1	1.5	2.0
	212.5	0.50	0.2	2.2	0.4	2.8	3.5
	212.6	0.75	0.4	3.4	0.7	4.5	5.6
	212.5	1.00	0.7	4.7	1.2	6.6	7.9
	212.3	2.00	2.5	10.3	4.1	16.9	18.7
	212.5	3.00	5.1	16.8	8.4	30.3	31.9
	212.6	3.50	6.7	20.5	11.1	38.3	39.4

ΔP_{us}: pressure drop in the capillaries located upstream of the column; ΔP_{col}: pressure drop across the chromatographic column; ΔP_{ds}: pressure drop across capillary located downstream of the column.

that the Blasius equation and the Darcy's law are suited for the prediction of pressure drop in SFC systems. The pressure profile in the chromatographic column calculated in this fashion was used for the predictions of the retention time and the efficiency.

5. Retention time

The retention time of phenanthrene in the SFC column was calculated by considering the dead time in the piping. Under conditions where the density of the fluid changes along the column, only the mass flow rate is constant along the column, as opposed to HPLC where the volumetric flow rate and the velocity are also constant. The measured values of the retention time at the two different temperature levels considered in this study are plotted in terms of mass flow rate in Fig. 2. Closed and open symbols correspond to experiments where the calculated density drop across the column was less and more than 3%, respectively.

For a given mass flow rate, a higher value of the back pressure corresponds to a smaller fluid velocity due to the higher density, which in turn causes a weaker retention of the solute. The former effect leads to larger retention times, whereas the latter in fact to smaller ones. From Fig. 2 it can be noted that at both temperatures levels, for a given mass flow rate the retention time decreases as the value of the back pressure increases. This shows that under the conditions studied, the retention time is controlled by retention (through the Henry constant, H_i; see below) more than by the fluid velocity.

For systems where the solute is present in rather dilute conditions, the adsorption behaviour can be described by the linear isotherm:

$$n_i^* = H_i c_i \tag{8}$$

where H_i represents the Henry constant. In SFC systems with significant pressure drop along the column, the fluid density varies, thus making the interstitial fluid velocity, v, and the Henry constant be functions of the axial position, i.e.,

$$H_i = H_i(\rho(z)) = H_i(z) \tag{9a}$$

$$v = v(\rho(z)) = v(z) \tag{9b}$$

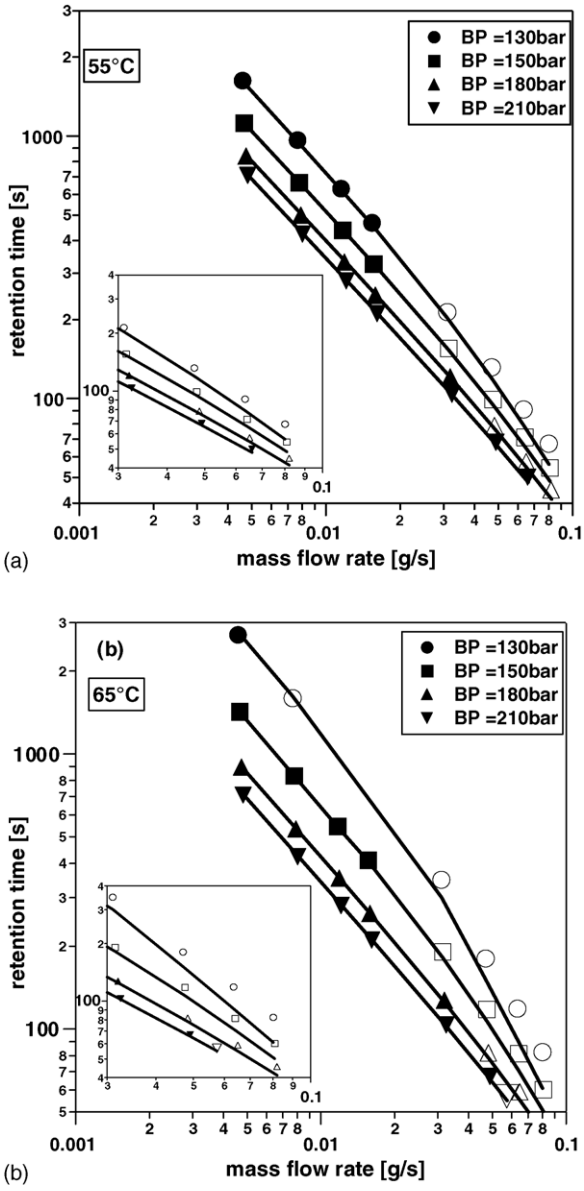

Fig. 2. Experimental (symbols) and calculated (lines) retention times at different back pressures (BP) at (a) 55 °C and (b) 65 °C. Closed symbols correspond to runs where the density drop across the column was less than 3%, whereas the open symbols correspond to those where the density drop was more than 3%. A zoom of the high flow rate region is shown in the inset.

Therefore, the retention time of a solute, t_i^R, is given by

$$t_i^R = \int_0^L \frac{1}{v(z)} \left(1 + \frac{1-\epsilon_b}{\epsilon_b} H_i(z)\right) dz \quad (10)$$

Hence, under these conditions, the experimentally measured retention times are due to the combined effect of the change of velocity and Henry constant along the column. However, in cases where the pressure drop is small, hence the density difference between the inlet and the outlet of the column is negligible, the following approximations can be made:

$$\rho(z) \simeq \bar{\rho} \quad (11a)$$

$$v(z) \simeq v(\bar{\rho}) \quad (11b)$$

$$H_i(z) \simeq H_i(\bar{\rho}) \quad (11c)$$

where $\bar{\rho}$ is the average density in the column. Incorporating these assumptions into Eq. (10) yields:

$$t_i^R = \frac{L}{v(\bar{\rho})} \left[1 + \frac{1-\epsilon_b}{\epsilon_b} H_i(\bar{\rho})\right] \quad (12)$$

and allows the Henry constant of the solute corresponding to the average density, $\bar{\rho}$, from the experimental retention time. In this study, those experimental runs which exhibited a density difference between the column inlet and outlet of less than 3% were considered to satisfy the assumptions made in Eq. (11). The Henry constants obtained from these runs are plotted in Fig. 3 as a function of the mobile phase density.

The density dependence of the Henry constant can be described by the following functional relationship:

$$H_i = r_i \rho^{b_i} \quad (13)$$

This expression can be derived theoretically for dilute systems [11,12] and has been shown to represent accurately SFC systems [2,13]. A plot of $\ln(H_i)$ versus $\ln(\rho)$ yielded a straight line and the values of the constants r_i and b_i obtained from the intercept and the slope, respectively, are shown in Table 3. The results obtained in this way are illustrated in Fig. 3, where it can be observed that, under the experimental conditions studied and for a given density, the Henry constant values at 55 °C are larger than the ones at 65 °C, as expected since adsorption is typically an exothermic process.

The information about the density profile, hence about the variation of the Henry constant along the column can be used to predict the retention time at conditions where the density drop is non-negligible. The integral of Eq. (10) can be solved numerically by using the local density value and

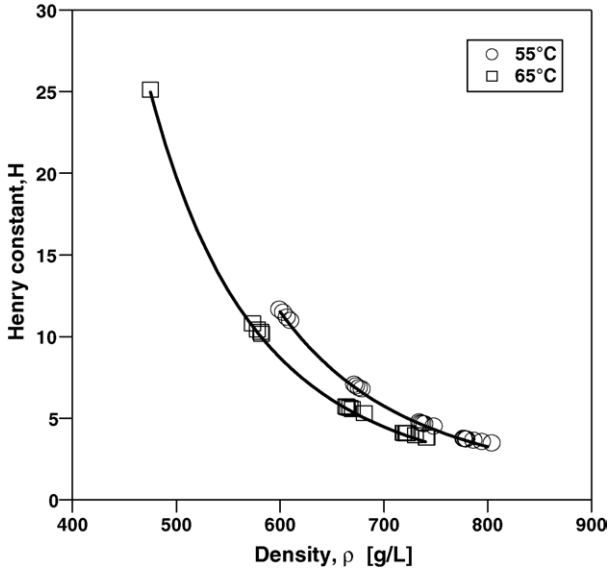

Fig. 3. Experimental (points) and fitted (lines) values of the Henry constant of phenanthrene as a function of fluid phase density at 55 and 65 °C.

Table 3
Values of r_i and b_i extracted from experimental runs with negligible pressure drop

	ln r	b
55 °C	32.9	−4.67
65 °C	32.6	−4.62

the corresponding Henry constant given by Eq. (13). The results of such a prediction along with the experimental results are shown in Fig. 2. At low flow rates the predictions match very well with the experimental retention times. At higher flow rates, the predicted retention times are always smaller than the experimental values. Moreover, at both temperatures the prediction of retention times is better at higher than at lower back pressure levels. This behaviour can be interpreted by considering a possible temperature drop along the column due to the expansion of the supercritical mobile phase. Though not investigated in the present study, such an effect is plausible and has been reported elsewhere [14,15]. This effect has been demonstrated experimentally wherein temperature drops upto 5 °C were observed for pressure drops of about 20 bar. In the present study, the pressure drops measured were much larger and hence could lead to higher temperature differences. It is to be noted that the effect of expansion of the mobile phase would be significant under conditions where the CO_2 is compressible, and therefore the effects of the temperature drop across the column are expected to be more significant at lower pressures than at higher pressures. If this were the case, density in the last portion of the column would be larger than that predicted by the isothermal model adopted in this study. A larger value of density leads to a lower value of the fluid velocity which will cause an increase in the retention time. As discussed before since the retention is also a function of the fluid phase density, the Henry constant is also bound to change. However, depending on the degree of temperature change and the corresponding change in the density, the two effects that affect the retention times, i.e., the change in velocity and the change in the Henry constant, could act in a fashion so as either to increase the retention time or to decrease it. This could be determined by studying and characterizing variations along the column, which was beyond the scope of this work. However, for practical reasons, the predictions are rather good and this model can be successfully employed to model retention times in preparative systems.

6. Efficiency

Mass transfer in chromatographic columns can be characterized by the height equivalent to a theoretical plate, HETP, defined as

$$\mathrm{HETP} = L\frac{\sigma_i^2}{(t_i^{\mathrm{R}})^2} = \frac{L}{N} \tag{14}$$

where σ_i^2 is the second moment of the chromatographic pulse response, L is the column length and N is the number of theoretical plates. The latter parameter is obtained from an experimental chromatogram as:

$$N_{\mathrm{expt}} = 5.545\left(\frac{t_i^{\mathrm{R}}}{w_i}\right)^2 \tag{15}$$

where w_i is the peak width at half peak height. Under linear conditions, it is customary to plot the HETP against the fluid phase velocity to obtain the Van Deemter curve, which is described by the Van Deemter equation:

$$\mathrm{HETP} = A + \frac{B}{v} + Cv \tag{16}$$

where the first term represents the contribution of eddy diffusion; the second that of molecular diffusion, $D_{\mathrm{m},i}$; and the third that of mass transfer resistance.

In the case of HPLC, for a given flow rate, the fluid phase velocity is constant throughout the column. Operating the system with different flow rate causes changes in the fluid velocity alone, while all other retention and kinetic properties remain unchanged. Thus, the Van Deemter curve clearly shows the effect of changing the fluid phase velocity alone. However, in SFC systems under conditions of non-negligible pressure drop, all properties including the fluid phase velocity vary along the length of the column. Thus, under these conditions, plotting the Van Deemter curve in the conventional way does not truly represent the effect of the fluid phase velocity alone. However, for the want of a convenient method to visualize the data, the HETP curves can be grouped according to the back pressure levels and plotted as a function of the mass flow rate, the only invariant parameter along the column. It is worth noting that for a given back pressure setting, varying the mass flow rates will produce a different pressure profile in the column, thus leading to different inlet conditions. Hence, the Van Deemter plot used in this fashion should be treated only in a qualitative sense.

Fig. 4(a) and (b) show the Van Deemter plots for the experimental runs at 150, 180, and 210 bar for the temperatures 55 and 65 °C, respectively. The curves in Fig. 4(a) and (b) have the familiar shape of a typical Van Deemter curve, which at low velocities decrease with increase in velocity, reaches a minimum; and rises again. From Fig. 4(a) and (b), it can be observed that the influence of pressure level on the HETP values is minor. Hence, for convenience, the HETP dependence on the mass flow rate can be averaged as shown by the dotted line. This averaged HETP curve is compared with the HETP curve at 130 bar in the inset of the Fig. 4(a) and (b). At 55 °C, the difference between the two curves is minimal and for a given mass flow rate, the curve corresponding to a back pressure level of 130 bar has a higher value compared to the other curve. However, at 65 °C, at flow rates above 0.02 g/s, the HETP increases sharply with the increase in mass flow rate and shows a substantial difference with the averaged HETP curve. In order to ascertain that the observations at 130 bar are not experimental artifacts, a set of runs at a back pressure level of 135 bar was performed. The HETP values at a back

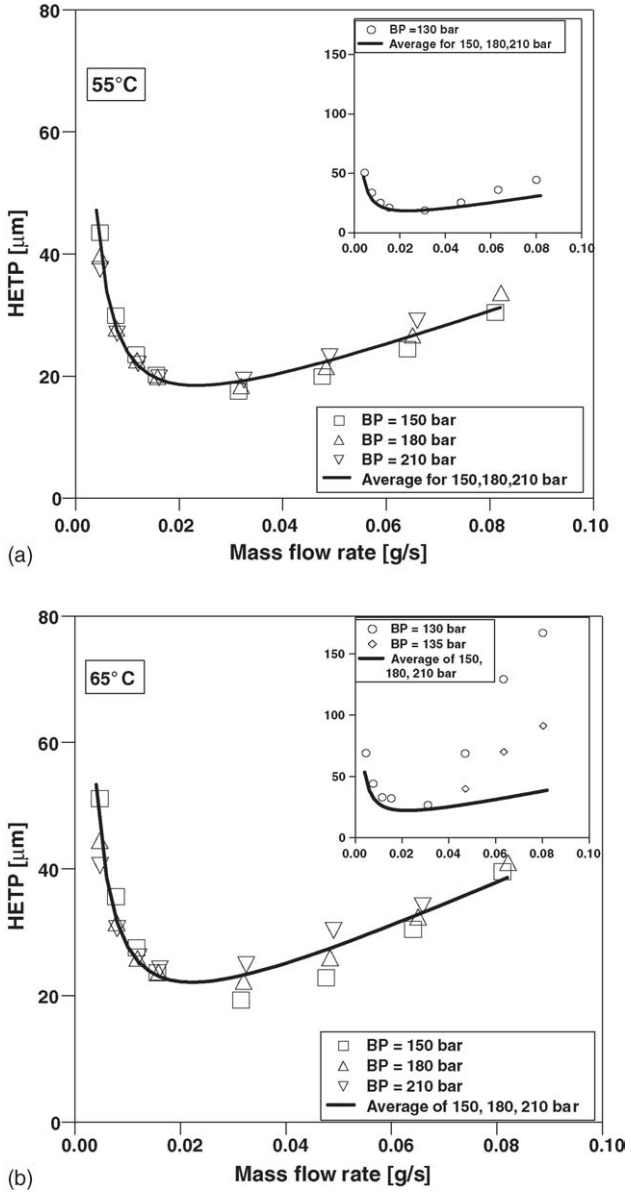

Fig. 4. Experimental HETP curves at different back pressures at (a) 55 °C and (b) 65 °C. The solid line represents the average of HETP values at back pressure levels 150, 180, and 210 bar. A comparison of this averaged value with runs at lower back pressure levels is shown in the inset.

pressure level of 135 bar, nicely fall between those at 130 bar and the averaged HETP curve thus confirming the correctness of the results at a back pressure of 130 bar. The possibility of a temperature drop along the column can be invoked to explain this behavior. A drop in the temperature leads in fact to an increase in retention time and to lower values of diffusivity, both of which tend to increase the HETP.

In SFC systems operated under non-negligible pressure drop conditions, the measured HETP represents the combined effect of the physical properties that vary along the column. Under such a situation, the following strategy has been adopted to account for the local variations of the physicochemical properties. First the column is divided into several small lengths within which the physicochemical properties can be assumed to be constant. Then, an expression to describe the HETP over this element is written in terms of the second moment. Finally the additivity of the second moment is invoked to calculate the second moment of the entire column and hence the overall HETP. This is described below.

Consider a sufficiently small length of the column Δz at an axial position z from the inlet of the column, within which the physicochemical properties can be assumed to be constant. For this small length the expression to calculate HETP, as in Eq. (14) can be written as:

$$\frac{\mathrm{HETP}(z)}{\Delta z} = \frac{\Delta\sigma_i^2(z)}{[\Delta t_i^{\mathrm{R}}(z)]^2} \tag{17}$$

which can be rearranged to give

$$\Delta\sigma_i^2(z) = \frac{\mathrm{HETP}(z)}{\Delta z}[(\Delta t_i^{\mathrm{R}}(z))]^2 \tag{18}$$

The retention time, $\Delta t_i^{\mathrm{R}}(z)$, is given by

$$\Delta t_i^{\mathrm{R}}(z) = \frac{\Delta z}{\omega(z)} \tag{19}$$

where $\omega(z)$ is the wave velocity of the concentration front at the location z, i.e.,

$$\omega(z) = \frac{v(z)}{(1 + ((1-\epsilon_{\mathrm{b}})/\epsilon_{\mathrm{b}})H_i(z))} \tag{20}$$

Combining Eqs. (18) and (19), with $\Delta z \to 0$ one obtains:

$$\mathrm{d}\sigma_i^2 = \frac{\mathrm{HETP}(z)}{(\omega(z))^2}\,\mathrm{d}z \tag{21}$$

Since σ_i^2 is additive, the above equation can be integrated to obtain $[\sigma_i^2]_{\mathrm{col}}$, the second moment of the pulse response of the chromatographic column:

$$[\sigma_i^2] = \int_0^L \frac{\mathrm{HETP}(z)}{(\omega(z))^2}\,\mathrm{d}z \tag{22}$$

Combining Eqs. (10), (14) and (22) one obtains the expression to calculate the HETP representative of the entire column given by

$$\mathrm{HETP} = L\frac{[\sigma_i^2]_{\mathrm{col}}}{(t_i^{\mathrm{R}})^2} = \frac{L}{(t_i^{\mathrm{R}})^2}\int_0^L \frac{\mathrm{HETP}(z)}{(\omega(z))^2}\,\mathrm{d}z \tag{23}$$

The HETP value obtained by using Eq. (23) can then be compared to the experimentally measured value given in Eq. (14).

Eq. (23) gives the general relation to calculate the HETP for the entire chromatographic column. In order to calculate the HETP, a suitable mass transfer model has to be adopted which takes into account the contributions of axial dispersion and mass transfer resistance to the HETP. As discussed before the Van Deemter equation can be used to calculate the value of the HETP:

$$\mathrm{HETP}(z) = A + \frac{B(z)}{v(z)} + C(z)v(z) \tag{24}$$

The term A corresponds to the contribution of eddy diffusion and is a function of the particle diameter, d_p

$$A = 2\gamma_2 d_p \tag{25}$$

where γ_2 is an empirical constant. The second term in the equation corresponds to the contribution of molecular diffusion to axial dispersion and is given by

$$B(z) = 2\gamma_1 D_{m,i}(z) \tag{26}$$

where γ_1 is an empirical constant. The terms involving A and B are combined and expressed as the axial dispersion coefficient, $D_{ax,i}(z) = (\gamma_1 D_{m,i}(z) + \gamma_2 d_p v(z))$. Unlike liquids and gas systems, there are fewer studies on the axial dispersion in supercritical fluids [16,17]. In most instances, a better method would be to obtain information from the HETP curves of the system under investigation as adopted in this work. The third term in Eq. (24), describes the contribution of the mass transfer resistance to the HETP. The transfer of the solute from the mobile phase to the solid phase occurs through several resistances, namely the resistance of the fluid film around the particle, the diffusional resistance in the pores filled with the mobile phase and the resistance arising due to the kinetics of adsorption. In this study, it was assumed that the mass transfer resistance arises chiefly from two factors, namely the fluid film, which is characterized by the film mass transfer coefficient, $k_{f,i}$, and the diffusion in the pore, characterized by the pore diffusion coefficient, $D_{p,i}$. Under these assumptions the factor:

$$C(z)=2\left(\frac{1-\epsilon_b}{\epsilon_b}\right)\frac{1}{k_i(z)H_i(z)}\left(1+\frac{\epsilon_b}{(1-\epsilon_b)H_i(z)}\right)^{-2} \tag{27}$$

Combining Eqs. (25)–(27) the expression to calculate the HETP is given by

$$\begin{aligned}\mathrm{HETP}(z) = {} & \frac{2\gamma_1 D_{m,i}(z)}{v(z)} \\ & + 2\gamma_2 d_p + 2v(z)\left(\frac{\epsilon_b}{1-\epsilon_b}\right)\frac{1}{k_i(z)H_i(z)} \\ & \times \left(1+\frac{\epsilon_b}{(1-\epsilon_b)H_i(z)}\right)^{-2}\end{aligned} \tag{28}$$

In the above equation the molecular diffusion coefficient, $D_{m,i}$, is calculated by using a correlation proposed by Akgerman et al. [18] for phenanthrene-CO_2 system:

$$D_{m,i}(z) = 1.2525\times 10^{-5}\sqrt{T}(\bar{V}(z)^{0.2126} - V_0^{0.2126}) \tag{29}$$

where $\bar{V}$ is the molar volume of the solvent and the close packed molar volume, $V_0 = 18.83\,\mathrm{cm}^3/\mathrm{mol}$. The lumped mass transfer coefficient, $k_i(z)$ can be calculated by adding the resistance to mass transfer from the fluid film surrounding the particle and the diffusional resistance in the pores filled with the solvent:

$$\frac{1}{k_i(z)H_i(z)} = \frac{d_p}{6k_{f,i}(z)} + \frac{d_p^2}{60\epsilon_p D_p(z)} \tag{30}$$

Table 4
Fitted values of γ_1 and γ_2 by different methods

	55 °C		65 °C	
	γ_1	γ_2	γ_1	γ_2
Method A	0.93	1.27	0.93	1.27
Method B	0.85	1.12	0.81	1.57

Method A corresponds to determining the values by fitting them over both the temperatures, while Method B refers to fitting them independently at 55 and 65 °C.

where ϵ_p is the particle porosity, which was assumed to be 0.46, thus yielding $\epsilon_b = 0.35$. It is worth noting that for this type of bi-disperse particles the Henry constant is defined as $H_i = \epsilon_p + (1-\epsilon_p)K_i$ where K_i is an adsorption equilibrium constant. The value of $k_{f,i}$ was estimated using an empirical correlation [19]

$$\frac{d_p k_{f,i}(z)}{D_{m,i}(z)} = 2.0 + 1.1\left(\frac{\mu(z)}{\rho(z)D_{m,i}(z)}\right)^{1/3}\left(\frac{d_p v(z)\rho(z)}{\mu(z)}\right)^{0.6} \tag{31}$$

The pore diffusion coefficient was calculated by the expression

$$D_p = \frac{D_{m,i}\epsilon_p}{\tau}F(\lambda) \tag{32}$$

where τ is the particle tortuosity, which was assumed to be 3.0, and $F(\lambda) = (1-\lambda)^4$ accounts for the restricted diffusion in the pores, with λ being the ratio of the molecular diameter to the pore diameter [20]. The value of λ for the phenanthrene – LiChrospher RP-18 system was 0.115. It is worth noting that both terms in Eq. (30) are important in the case of the system considered in this study, possibly due to the rather small particle size selected, i.e., 5 μm.

Integrating Eq. (23) after inserting Eq. (28) yields the expression for the HETP which can be compared to the experimentally measured one. It can be seen that in Eq. (28) there are two system dependent empirical parameters γ_1 and γ_2. Two methods were adopted to determine these empirical constants. In the first method called "Method A" these parameters were evaluated by considering them to be invariant with pressure and temperature, and in "Method B", they were considered to be dependent on temperature. In both the cases, the parameters were obtained by minimizing the sum of the residuals of the calculated and experimental HETP values at 150, 180, and 210 bar. The values of γ_1 and γ_2 are given in Table 4 and comparison of the experimental and calculated HETP values is shown in Fig. 5(a) and (b).It can be seen that at low flow rates both the methods predict the HETP behaviour well. However, at larger flow rates there is a difference in their predictions.

From the experiments and calculations, it can be seen that in the region where the mobile phase is less compressible, significant loss of efficiency due to pressure drop has not been observed. However, as demonstrated in the case of the runs at 130 bar, significant losses can be seen in the region where the mobile phase is more compressible. Evidence from the

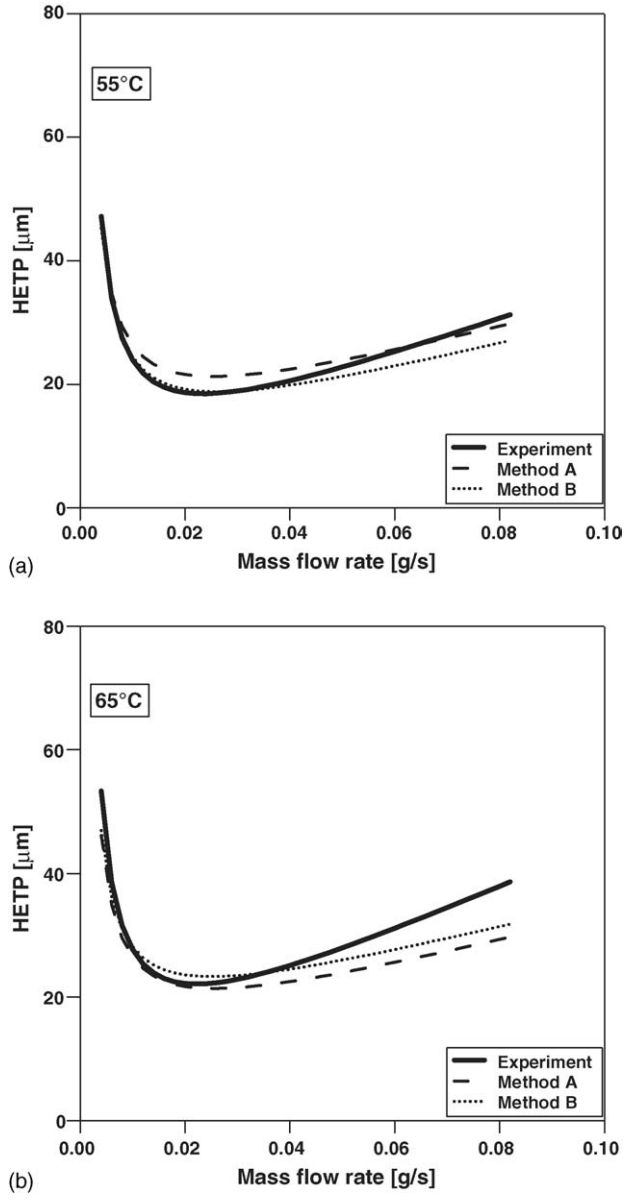

Fig. 5. Experimental and calculated HETP curves at different back pressures at (a) 55 °C and (b) 65 °C.

retention time predictions and the modeling of the efficiency suggest that a drop in temperature due to the expansion of the fluid phase can explain the observed differences. In order to account for this, an essential step would be to measure and properly account for possible temperature variations in the column due to the expansion of the mobile phase. These effects may not be significant in systems that use a modified mobile phases, since the addition of a modifier reduces the compressibility substantially.

7. Numerical simulation of chromatograms

The simulation of the response of a SFC column under non-negligible pressure drop conditions is the ultimate aim of this study. With the parameters estimated from the experiments, it is possible to solve numerically Eqs. (1)–(5) along with suitable initial and boundary conditions to yield the pulse response of the column. Under dilute conditions of the pulse, as explained before, the equation describing the hydrodynamics, namely Eqs. (1) and (2), can be solved independent of the solute material balance equations with P_{out} as the boundary condition. The Blasius and the Darcy equations, along with the EOS and the correlation for calculating the viscosity of CO_2, were used to calculate the pressure drop in the capillary and in the columns. The ordinary differential equations Eqs. (1) and (2) were solved using the method of orthogonal collocation with 120 internal collocation points [21] along with the equation of state and the viscosity correlation. The solution yielded the profile of the physicochemical properties along the column.

Using the information obtained by solving Eqs. (1) and (2), it is possible to solve Eqs. (3)–(5), which describe the transport of the pulse of solute along the column. In addition to the hydrodynamic properties, information concerning the isotherm, in the form of Eq. (13), along with the expression for axial dispersion and the linear driving force coefficient, k_i, were used for the simulation. The set of algebraic and partial differential equations were combined with suitable initial and boundary conditions. The orthogonal collocation method was used to discretize the partial differential equations in space, while the Gear's method was used to integrate the discretized equation in time. The equations were solved and the response to a pulse input of the solute was simulated.

Two operating conditions were considered to compare the experimental and simulated chromatograms. The first condition corresponded to a situation where the predicted retention times and the HETP values were in good agreement with the experimental values. The experimental run chosen for the comparison was the one at 55 °C, back pressure of 150 bar, and a CO_2 flow rate of 2.0 cm^3/min at the pump, i.e., a mass flow rate of 0.031 g/s. The comparison of the pulse responses, normalized to the area, is shown in Fig. 6(a). It can be seen that under these conditions, the prediction of both retention time and peak width is excellent.

In the second comparison, an experimental run with a high mass flow rate is chosen, namely at a temperature of 55 °C, a back pressure level of 150 bar, and a CO_2 flow rate of 5.0 cm^3/min, which corresponds to a mass flow rate of 0.081 g/s. The comparison of the normalized pulse is shown in Fig. 6(b). As expected by considering Fig. 2 the simulation predicts a shorter retention time for the peak as compared to the experimental one. It can also be seen that the peak in the case of the simulation is spread less, which is an indication of a lower value of HETP.

From these simulations it can be seen that by properly accounting for the pressure drops and the variation of the physicochemical properties along the column operated under non-negligible pressure drop conditions, the standard column dynamics model can be adopted to qualitatively and quantitatively predict pulse dynamics in SFC systems. At higher

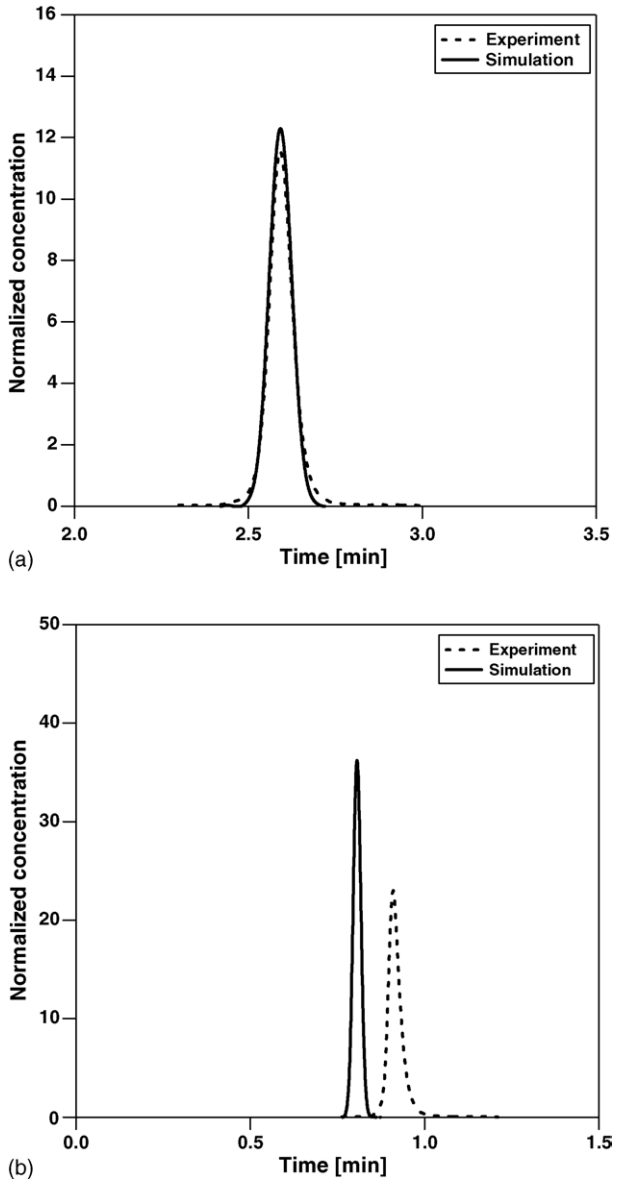

Fig. 6. Comparison of experimentally measured (dotted lines) and simulated (solid line) chromatograms of phenanthrene. The experimentally measured chromatogram has been normalized to the area of the calculated chromatogram, thereby eliminating the need for detector calibration. Operating conditions: (a) temperature, 55 °C; back pressure, 150 bar; mass flow rate, 0.031 g/s; (b) temperature, 55 °C; back pressure, 150 bar; mass flow rate, 0.081 g/s.

flow rates, it is suspected that temperature effects might play a role. In order to account for this effect, a non-isothermal model including heat-effects due to the expansion of the mobile phase must be considered.

8. Concluding remarks

The effect of pressure drop on the performance of SFC was studied with the aim of developing models for the simulation of preparative-SFC systems. The investigations were carried out on a LiChrospher RP-18 column with 5 μm particles, using phenanthrene as a solute and pure CO_2 as a mobile phase. The main parameters whose characterization are vital are the pressure drop, retention time an the efficiency. Experiments were performed at conditions where the solute was in a rather diluted state permitting the use of a linear adsorption isotherm. Four different back pressure levels, 130, 150, 180, and 210 bar at two different temperatures 55 and 65 °C were chosen for performing the experiments which spanned a range of flow rates, from those which produced negligible pressure drop to those where non-negligible pressure drops were observed.

Darcy's law was used to describe the pressure drop in the column. The parameters to describe the pressure drop was extracted from experiments over the entire flow rate range. The dependence of the Henry constant on the fluid phase density was obtained from experiments which offered negligible pressure drops. By combining the density profile and the dependence of the Henry constant on the fluid phase density, it was possible to calculate the retention time. Good predictions of the retention times were obtained at low and moderate flow rates. At higher values of mass flow rate, the prediction of the retention time for runs at higher back pressure levels was good. At lower levels of back pressure, the calculated retention times were slightly higher than the experimental ones. The efficiency of the column, characterized by the HETP yielded interesting results. At the back pressure levels of 150, 180, and 210 bar, running the system at high flow rates did not produce a considerable drop in efficiency. However at 65 °C and a back pressure level of 130 bar, substantial loss in efficiency was observed at high flow rates. Experiments at lower back pressure levels, showed further loss in efficiency. The mass transfer was modeled by using the parameters extracted from the experiments along with standard correlations and empirical constants fitted to the experimental data. From the model, the HETP values were predicted and were found to be in good agreement with the experimental ones at low flow rates while at larger flow rates, the predictions were satisfactory. The column model was solved numerically and the elution profiles were compared to the experimental chromatograms. The observed differences between the experimental and predicted values of the retention time and HETP were conjectured to arise from the drop of temperature due to the expansion of the fluids.

9. Nomenclature

A	parameter in Van Deemter equation (1/s)
b	Constant in the van Wasen type relationship between Henry constant and density
B	parameter in Van Deemter equation (μm)
c	concentration of a solute in the fluid phase (moles/cm^3)
C	parameter in Van Deemter equation (s)

d_p	particle diameter (cm)
D_{ax}	axial Dispersion coefficient (cm^2/s)
$D_{m,i}$	molecular diffusion coefficient (cm^2/s)
D_p	pore diffusion coefficient (cm^2/s)
G	mass flow rate (g/s)
H	Henry constant
HETP	Height Equivalent to a Theoretical Plate (μm)
k	lumped mass transfer coefficient (1/s)
K	adsorption equilibrium constant
L	length of chromatographic column (cm)
N	number of plates
P	pressure (bar)
n	solid phase concentration ($moles/cm^3$)
n^*	equilibrium solid phase concentration ($moles/cm^3$)
r	Constant in the van Wasen type relationship between Henry constant and density
t	time (s)
T	temperature (K)
v	interstitial velocity (cm/s)
V	molar volume (cm^3/mol)
V_a	close packed volume (cm^3/mol)
w	width of a chromatographic peak (s)
z	axial coordinate (cm)

Greek letters

α	parameter in Eq. (6) ($cm^{-19/4}$)
β	parameter in Eq. (1) (cm^{-4})
γ_1	parameter in Eq. (25)
γ_2	parameter in Eq. (26)
ϵ	bed porosity
ϵ_p	particle porosity
λ	ratio of molecular diameter of the solute to the pore diameter
μ	viscosity (g/(cm s))
ρ	density (g/L)
σ^2	standard deviation (s^2)
τ	particle tortuosity

Subscripts and superscripts

0	non-retained component
col	column
ds	downstream
expt	experimental
i	component
in	inlet
out	outlet
pred	predicted
R	retention
us	upstream

Acknowledgements

Partial support of the Swiss National Science Foundation through grant SNF 20-67989.02 is gratefully acknowledged.

References

[1] G. Terfloth, J. Chromatogr. A 906 (1–2) (2001) 301.
[2] F. Denet, W. Hauck, R.M. Nicoud, O. Di Giovanni, M. Mazzotti, J.N. Jaubert, M. Morbidelli, Ind. Eng. Chem. Res. 40 (21) (2001) 4603.
[3] S. Peper, M. Lubbert, M. Johannsen, G. Brunner, Sep. Sci. Technol. 37 (11) (2002) 2545.
[4] O. Di Giovanni, M. Mazzotti, M. Morbidelli, F. Denet, W. Hauck, R.M. Nicoud, J. Chromatogr. A 919 (1) (2001) 1.
[5] H.G. Janssen, H. Snijders, C. Cramers, P. Schoenmakers, HRC J. High Resolut. Chromatogr. 15 (7) (1992) 458.
[6] H.G. Janssen, H.M.J. Snijders, J.A. Rijks, C.A. Cramers, P.J. Schoenmakers, HRC J. High Resolut. Chromatogr. 14 (7) (1991) 438.
[7] X.W. Lou, H.G. Janssen, H. Snijders, C.A. Cramers, HRC J. High Resolut. Chromatogr. 19 (8) (1996) 449.
[8] C. Bouigeon, D. Thiebaut, M. Caude, Anal. Chem. 68 (20) (1996) 3622.
[9] R. Span, W. Wagner, J. Phys. Chem. Ref. Data 25 (6) (1996) 1509.
[10] A. Fenghour, W.A. Wakeham, V. Vesovic, J. Phys. Chem. Ref. Data 27 (1) (1998) 31.
[11] U. van Wasen, G.M. Schneider, Chromatographia 8 (6) (1975) 274.
[12] M. Perrut, J. Chromatogr. A 658 (2) (1994) 293.
[13] A. Rajendran, M. Mazzotti, M. Morbidelli, J. Chromatogr. A 1076 (2005) 183.
[14] D.P. Poe, J. Chromatogr. A 785 (1–2) (1997) 129.
[15] D.P. Poe, P.J. Marquis, T. Tomlinson, J. Dohm, J. He, J. Chromatogr. A 785 (1–2) (1997) 135.
[16] O.J. Catchpole, R. Bernig, M.B. King, Ind. Eng. Chem. Res. 35 (3) (1996) 824.
[17] T. Funazukuri, C.Y. Kong, S. Kagei, J. Supercrit. Fluids 13 (1–3) (1998) 169.
[18] A. Akgerman, C. Erkey, M. Orejuela, Ind. Eng. Chem. Res. 35 (3) (1996) 911.
[19] N. Wakao, T. Funazkri, Chem. Eng. Sci. 33 (10) (1978) 1375.
[20] C.N. Satterfield, C.K. Colton, W.H. Pitcher, AIChE J. 19 (3) (1973) 628.
[21] J.V. Villadsen, W.E. Stewart, Chem. Eng. Sci. 22 (11) (1967) 1483.